THE JOURNAL OF PHYSICAL CHEMISTRY B
A JOURNAL OF THE AMERICAN CHEMICAL SOCIETY

pubs.acs.org/JPCB

Article

Nonane and Hexanol Adsorption in the Lamellar Phase of a Nonionic Surfactant: Molecular Simulations and Comparison to Ideal Adsorbed Solution Theory

Published as part of The Journal of Physical Chemistry virtual special issue "Doros N. Theodorou Festschrift".

Mona S. Minkara,* Tyler R. Josephson, Connor L. Venteicher, Benjamin R. Greenvall, Rebecca K. Lindsey, Peter H. Koenig, and J. Ilja Siepmann*

Cite This: *J. Phys. Chem. B* 2022, 126, 3940−3949

Read Online

ACCESS | Metrics & More | Article Recommendations | Supporting Information

ABSTRACT: Adsorption of *n*-nonane/1-hexanol (C9/C6OH) mixtures into the lamellar phase formed by a 50/50 w/w triethylene glycol mono-*n*-decyl ether (C10E3)/water system was studied using configurational-bias Monte Carlo simulations in the osmotic Gibbs ensemble. The interactions were described by the Shinoda−Devane−Klein coarse-grained force field. Prior simulations probing single-component adsorption indicated that C9 molecules preferentially load near the center of the bilayer, increasing the bilayer thickness, whereas C6OH molecules are more likely to be found near the interface of the polar and nonpolar moieties, swelling the bilayer in the lateral dimension. Here, we extend this work to binary C9/C6OH adsorption to probe whether the difference in the spatial preferences may lead to a synergistic effect and enhanced loadings for the mixture. Comparing loading trends and the thermodynamics of binary adsorption to unary adsorption reveals that C9−C9 interactions lead to the largest enhancement, whereas C9−C6OH and C6OH−C6OH interactions are less favorable for this bilayer system. Ideal adsorbed solution theory yields satisfactory predictions of the binary loading.

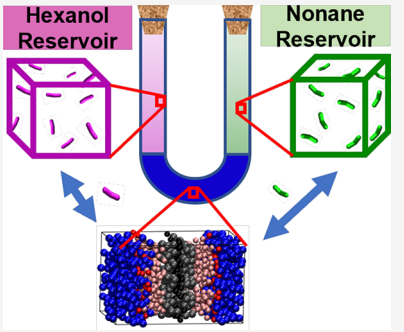

INTRODUCTION

Solute uptake in surfactant/solvent mesophases is a complex phenomenon due to cooperative and competitive effects. Many properties of the solute, such as solubility, polarity, shape, or rigidity, affect its uptake. Additionally, the number of favorable solute sorption domains that exist can be modified by solute uptake, leading to changes in local structure and global morphology.[1] Especially important to this work, these surfactant/solvent/solute systems only become more complicated when multiple solutes are introduced. Gaining insight into these more complex multisolute systems can help the understanding of many biologically and industrially relevant systems.[2−5]

Unary adsorption and absorption measurements are much more common than multicomponent measurements,[6] yet the ubiquity of mixtures in biological systems makes characterizing these multicomponent effects critical. Ideal Adsorbed Solution Theory (IAST) relates multicomponent adsorption to unary adsorption by assuming that the adsorbed phase is an ideal mixture and is a convenient, parameter-free method for treating mixture adsorption.[7] IAST has been shown to be a reasonable approximation in some systems,[8,9] but can fail when the adsorbed phase is not ideal (e.g., very strong adsorbate−adsorbate interactions).[10]

Experimental measurements[11−22] have provided a wealth of structural and thermodynamic information, such as the surfactant headgroup area, bilayer repeat distance, headgroup hydration, segmental order parameters, and partition coefficients for additives, but molecular-level information on the solute uptake and the solutes' spatial distribution is not yet available. Molecular dynamics simulations to investigate surfactant/solvent/solute systems are hampered by limitations imposed by closed systems that do not allow for controlling the chemical potential of the solutes.[23−32] Prior molecular simulations[33,34] utilizing open ensembles, that is, allowing for fluctuations in the numbers of solute molecules, have mostly focused on other properties of the surfactant system, such as the critical micelle concentration. A notable exception is the grand-canonical Monte Carlo simulations study by Rodgers et al.[35] that probed the solubility of a short-chain alcohol in a lipid bilayer using a coarse-grained model.

Received: February 17, 2022
Revised: April 30, 2022
Published: May 20, 2022

https://doi.org/10.1021/acs.jpcb.2c02871
J. Phys. Chem. B 2022, 126, 3940−3949

In previous work, we utilized Gibbs ensemble Monte Carlo (GEMC) simulations[36] to examine the solute loading and spatial distribution separately for *n*-nonane (C9) and 1-hexanol (C6OH) additives into a 50/50 w/w triethylene glycol mono-*n*-decyl ether (C10E3)/water system, forming a lamellar mesophase with a surfactant bilayer.[37] An important finding of our prior simulation study is the different spatial loading preferences for the C9 and C6OH molecules. That is, the nonpolar C9 molecules preferentially adsorb near the center of the surfactant bilayer, and this adsorption results in an increase of the bilayer thickness, but does not affect the surfactant headgroup area. In contrast, the amphiphilic C6OH molecules are more likely to be found near the interface of the polar (formed by surfactant ether groups and intruding water molecules) and nonpolar moieties (formed by surfactant decyl tails), and this leads to a lateral swelling of the bilayer. Here, we extend the prior work to binary uptake to assess whether the different spatial preferences of nonpolar and amphiphilic solutes lead to synergistic uptake beyond that expected from unary adsorption. As illustrated in Figure 1, we

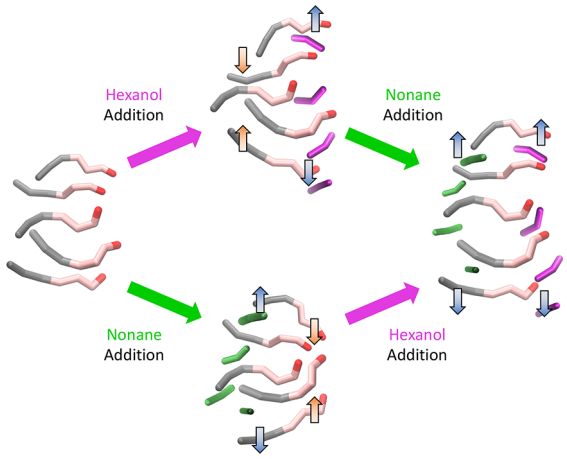

Figure 1. Schematic drawing illustrating the main hypothesis of this study. Loading of C6OH into the headgroup region of the C10E3 surfactants or loading of C9 into the tail group region causes inhomogeneous swelling and induces curvature strain on the lamellar mesophase. Addition of the complementary additive would relieve this strain and favor enhanced coadsorption.

hypothesize that adsorption of only one type of additive in a bilayer formed by amphiphiles with similar cross sections for head and tail groups imposes a curvature strain due to inhomogeneous swelling and that this strain can be relieved when a second type of additive with complementary spatial loading preference is adsorbed. This indirect curvature-strain-relief mechanism for synergistic adsorption would not require any specially favorable interactions between the two types of additives. Although strong favorable interactions would obviously lead to synergistic adsorption (and could be achieved by changing only the cross-interaction terms in a molecular simulation), we do not consider them in this work because, given the amphiphilic nature of the surfactants and the presence of water, it is likely that such a strong direct interaction would also alter the spatial loading preferences of the two types of additives. The simulation conditions cover the range from fairly low to high solute loadings (0.04 to 1 additive molecule per C10E3 molecule).

COMPUTATIONAL METHODS

Here we use Monte Carlo simulations in the osmotic version of the Gibbs ensemble[36] to study the binary uptake of C9 and C6OH into the lamellar phase formed by a 50/50 w/w C10E3/water mixture. Specifically, we use a three-box setup consisting of the surfactant/water mesophase simulation box in thermodynamic contact with two separate vapor-phase reservoir boxes containing either C9 or C6OH. The Monte Carlo for Complex Chemical Systems−Minnesota (MCCCS−MN) software suite was used for all simulations in this work.[38] All molecule types were modeled using the Shinoda−Devane−Klein (SDK) coarse-grained force field[39−41] (see Table 1 for

Table 1. Molecules and SDK Structure

molecule	SDK formula	SDK bead	chemical formula
n-nonane	CT−CM−CT	CT	CH_3-CH_2-CH_2−
1-hexanol	CT2−CM−OA	CM	−CH_2-CH_2-CH_2−
		CT2	CH_3-CH_2-
		OA	HO-CH_2−
C10E3	CT−$(CM)_2$−$(EO)_3$−OA	EO	−CH_2-O-CH_2−
water trimer	W	W	$[H_2O]_3$

the SDK representation of the molecules and Tables S1−S3 for the force field parameters). The SDK force field requires the use of a 15 Å cutoff without tail corrections (which is ideal for mesophases with heterogeneous bead densities). The SDK model offers significantly higher computational efficiency when compared to united-atom or all-atom force fields because it reduces the number of interaction sites by a factor of 2 (e.g., CT2 bead vs two united-atom beads) to about 10 (e.g., CT bead versus all-atom model or W bead vs 3-site or 4-site water models) and does not include long-range electrostatic interactions. However, there is a loss in accuracy compared to united-atom or all-atom force fields. Although the saturated vapor pressure at T = 300 K of C9 for the SDK model (p_{C9}^0 = 0.609 ± 0.003 kPa) is very accurate with a deviation of less than 2%,[37] the saturated vapor pressure of C6OH for the SDK model (p_{C6OH}^0 = 3.04 ± 0.01 kPa) is overpredicted by a factor of 22.[37] That is, judged solely by the vapor pressure, the SDK model for C6OH behaves like 1-propanol (for which the deviation would be less than 5%).[42] The ratio of the well depth parameters for the nonpolar CT, CM, and CT2 SDK beads appear reasonable, and we surmise that the strong over-prediction for C6OH is mostly caused by the OA−OA well depth, falling in between CT−CT and CM−CM, being too weak to account for the influence of hydrogen-bonding on the alcohol vapor pressure. However, the OA−W interaction is stronger.

The PACKMOL utility[43] was used to initialize the mesophase box with 100 C10E3 surfactant molecules and 538 water beads (where each bead represents three water molecules) arranged in a lamellar structure with a bilayer parallel to the *xy*-plane (with 50 molecules in each leaflet) and the polar headgroup of the surfactants pointing toward the water region. The initial dimension of the *xy*-plane (with $x = y$) was set to match the experimentally determined area per headgroup,[14] and the *z*-dimension was selected to yield a reasonable density. The two reservoir phases with cubic simulation boxes were initialized with 100 molecules each, and the ideal gas law was used to estimate the initial volumes.

https://doi.org/10.1021/acs.jpcb.2c02871
J. Phys. Chem. B 2022, 126, 3940−3949

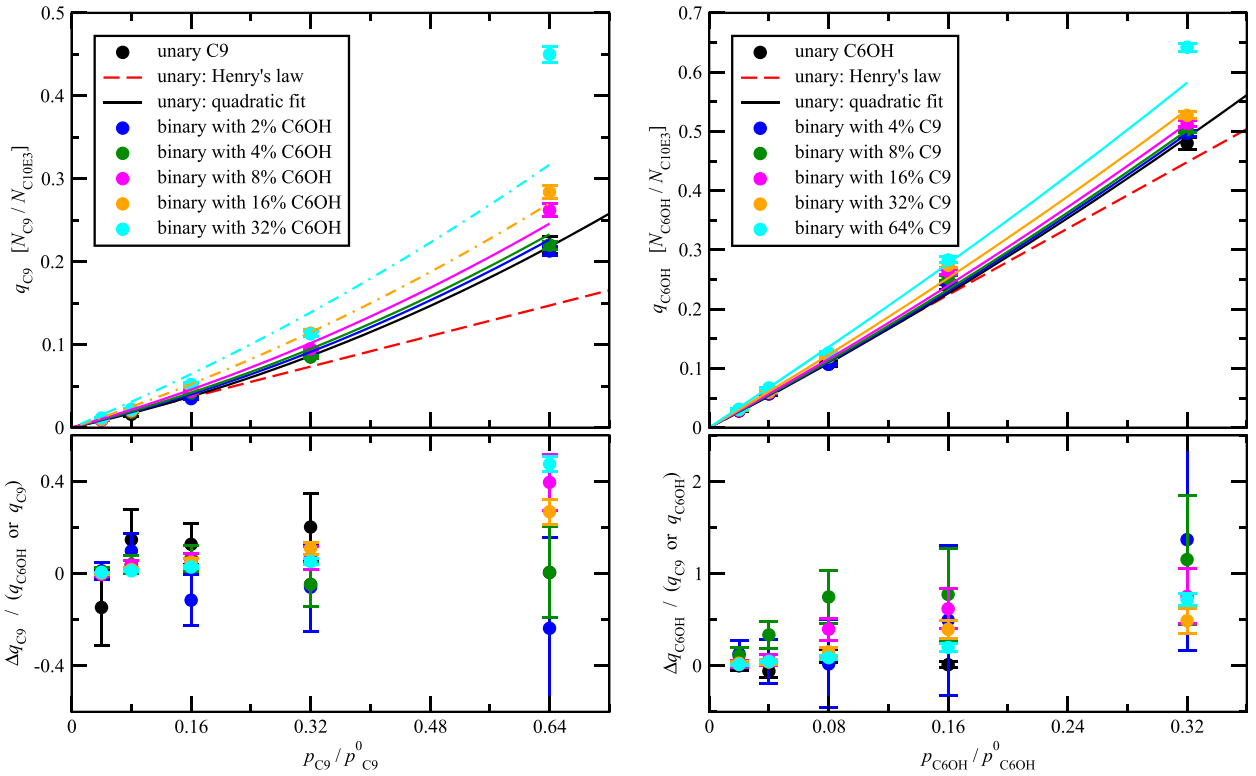

Figure 2. (Top) Loading of *n*-nonane (left) and 1-hexanol (right) solutes into the C10E3/water mesophase. Simulation data for unary adsorption are shown as black circles, and the corresponding Henry's law and quadratic isotherm fits are shown as red dashed and black solid lines, respectively. Simulation data for binary adsorption are shown as blue, green, magenta, orange, and cyan symbols (in order of increasing relative pressure of the other solute), and the corresponding IAST predictions are shown as solid lines or dash-dotted lines for extrapolative IAST predictions of the same color. (Bottom) Incremental loading of *n*-nonane (left) and 1-hexanol (right) normalized by the loading of the other component or pseudocomponent (see text). Error bars represent the standard error of the mean.

To obtain the binary loading isotherms, simulations were run in the $N_W N_{C10E3} N_{C9} N_{C6OH} p_{C9} p_{C6OH} p_{meso} T$ osmotic Gibbs ensemble with three simulation boxes, where the subscript "meso" refers to the surfactant/water mesophase, at T = 300 K, p_{meso} = 101 kPa, and 25 combinations of p_{C9} and p_{C6OH}, the pressures for the C9 and C6OH reservoirs. Based on differences in the unary loadings,[37] p_{C9} ranged from 0.04 to $0.64p^0_{C9}$ and p_{C6OH} ranged from 0.02 to $0.32p^0_{C6OH}$. Since the compressibility factors of the saturated vapor phases are near unity ($Z_{C9} > Z_{C6OH} > 0.997$),[37] intermolecular interactions were turned off in the two reservoir boxes. Molecules in all three boxes were allowed to translate and, with the exception of the one-site water model, rotate and undergo conformational changes. The volumes of the three boxes were allowed to vary independently subject to the corresponding thermodynamic constraints. Isotropic volume moves were performed for the two reservoirs. For the mesophase, the volume move involved a change in either the lateral area (i.e., coupled change in the *x*- and *y*-dimensions) or the thickness in the *z*-dimension with the corresponding scaled displacements in the center-of-mass coordinates of all molecules. The C9 and C6OH molecules were allowed to transfer only between their reservoirs and the mesophase. The efficiency of conformational changes and molecule transfers was enhanced through the configurational-bias Monte Carlo (CBMC) approach.[44,45] The frequencies of the different move types were adjusted to yield, on average, one accepted volume move and about 0.2 accepted particle transfer moves per Monte Carlo (MC) cycle, where a cycle consists of $N_W + N_{C10E3} + N_{C9} + N_{C6OH} = 838$ randomly selected MC moves. The remaining moves were divided equally between conformational, translational, and rotational moves.

At all 25 state points, simulation trajectories of at least 2000000 MC cycles were used for equilibration. Toward the end of these long equilibration periods, 12 independent trajectories were spawned using different random number seeds at each state point and equilibrated for another 200000 MC cycles. Production periods of 1000000 MC cycles were carried out for each of the 12 independent trajectories at each of the 25 state points. Statistical uncertainties are reported as the standard error of the mean estimated from the 12 independent trajectories.

RESULTS AND DISCUSSION

Solute Uptake and Thermodynamic Analysis. In our prior work probing unary adsorption,[37] we found that the loading of C6OH at the same relative pressure is, on average, roughly 6× greater than that of C9 (see Figure 2), but this difference largely reflects the ratio of saturated vapor pressures for the SDK models ($p_{C6OH}{}^0/p_{C9}{}^0 \approx 5$). With increasing pressure, the uptakes of both C9 and C6OH show a positive deviation from Henry's law behavior that is usually taken as an indication for additive−additive (or guest−guest) interactions being more favorable than additive−surfactant (or guest−host) interactions. It should be noted here that Rodgers et al.[35] found negative deviations from Henry's law behavior for the adsorption of a short-chain alcohol in a lipid bilayer.

https://doi.org/10.1021/acs.jpcb.2c02871
J. Phys. Chem. B 2022, 126, 3940−3949

Table 2. Thermodynamic Data for Binary Uptake[a]

p_{C9}*	p_{C6OH}*	V_{meso}	q_{C9}^{binary}	q_{C6OH}^{binary}	q_{C9}^{IAST}	q_{C6OH}^{IAST}	$\Delta G_{C9}^{vap\rightarrow meso}$	$\Delta G_{C6OH}^{vap\rightarrow meso}$
0.04	0.02	96.64_5	0.0097_5	0.0295_9	0.0090	0.0269	-18.55_{20}	-19.05_{13}
0.04	0.04	97.19_6	0.0098_5	0.057_1	0.0096	0.054	-18.63_{22}	-18.98_8
0.04	0.08	98.10_7	0.0089_4	0.107_2	0.0105	0.111	-18.37_{13}	-18.82_6
0.04	0.16	100.9_1	0.0098_5	0.244_3	0.0122*	0.230	-18.59_{17}	-19.00_5
0.04	0.32	105.9_2	0.0116_5	0.497_5	0.0153*	0.496	-18.77_{16}	-18.93_5
0.08	0.02	96.95_4	0.0191_8	0.0301_9	0.0187	0.027	-18.43_{16}	-19.06_9
0.08	0.04	97.53_6	0.0185_8	0.062_1	0.0198	0.055	-18.35_{14}	-19.19_7
0.08	0.08	98.72_9	0.0202_9	0.119_2	0.0217	0.112	-18.54_{10}	-19.01_7
0.08	0.16	101.4_2	0.0205_9	0.252_4	0.0251*	0.233	-18.56_{12}	-19.08_7
0.08	0.32	106.4_1	0.0222_8	0.503_5	0.0312*	0.502	-18.65_{10}	-18.98_3
0.16	0.02	97.37_8	0.035_1	0.0290_9	0.040	0.0284	-18.31_{16}	-19.03_{10}
0.16	0.04	98.15_7	0.042_1	0.059_1	0.042	0.057	-18.75_{11}	-19.07_6
0.16	0.08	99.43_9	0.044_2	0.122_2	0.046	0.116	-18.91_{11}	-19.05_5
0.16	0.16	102.4_1	0.050_2	0.263_4	0.053*	0.240	-19.10_{09}	-19.12_4
0.16	0.32	107.5_2	0.052_2	0.513_5	0.065*	0.514	-18.91_{14}	-19.00_4
0.32	0.02	98.9_1	0.086_2	0.0306_9	0.091	0.0304	-18.78_{11}	-19.02_8
0.32	0.04	99.4_1	0.085_2	0.060_1	0.095	0.061	-18.76_{13}	-19.09_7
0.32	0.08	100.9_1	0.095_2	0.120_2	0.102*	0.123	-18.91_9	-18.99_5
0.32	0.16	104.5_1	0.114_4	0.274_4	0.115*	0.252	-19.39_8	-19.21_3
0.32	0.32	109.5_3	0.113_3	0.527_6	0.139*	0.537	-19.12_8	-18.96_5
0.64	0.02	102.5_3	0.213_5	0.0310_9	0.227*	0.0339	-19.12_{10}	-19.05_{12}
0.64	0.04	103.5_4	0.220_5	0.067_1	0.233*	0.068	-19.14_{14}	-19.19_6
0.64	0.08	105.5_2	0.262_8	0.126_3	0.246*	0.136	-19.50_5	-19.05_7
0.64	0.16	109.4_6	0.284_8	0.283_5	0.271*	0.277	-19.72_{13}	-19.12_4
0.64	0.32	122_1	0.45_1	0.642_7	0.32*	0.582	-20.57_{13}	-19.24_3

[a]Volume of the mesophase (in nm^3), adsorption loadings (given as N_{solute}/N_{C10E3}) obtained from molecular simulation (q_{solute}^{binary}) and predicted by IAST (q_{solute}^{IAST}, where data with stars denote isotherm extrapolation), and Gibbs free energies of transfer (in kJ/mol). The subscripts denote the standard error of the mean given for the last digit(s).

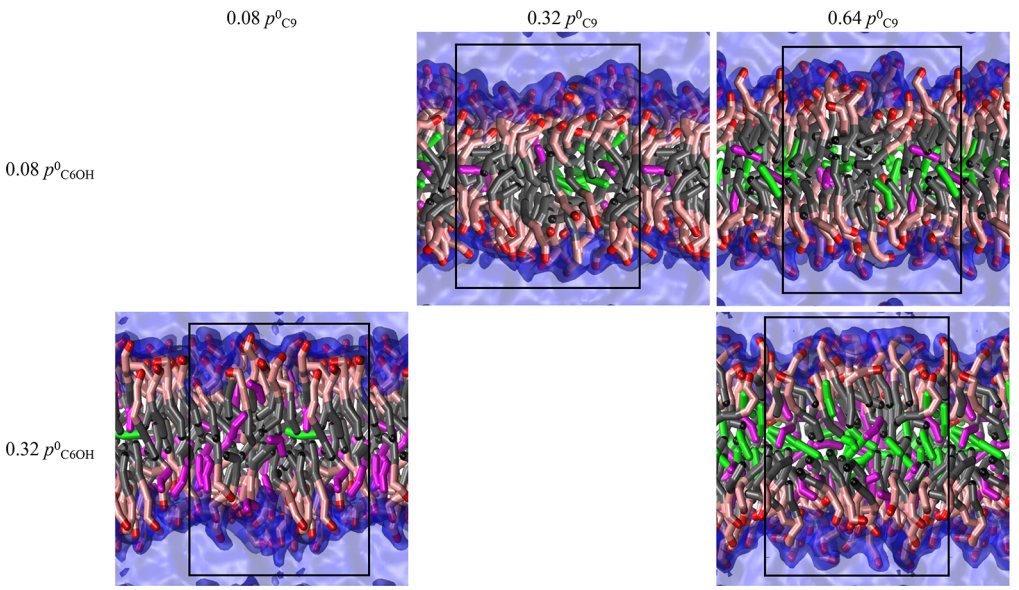

Figure 3. Snapshots of equilibrium configurations for systems at $0.32p^0_{C9} + 0.08p^0_{C6OH}$ (top middle), $0.64p^0_{C9} + 0.08p^0_{C6OH}$ (top right), $0.08p^0_{C9} + 0.32p^0_{C6OH}$ (bottom left), and $0.64p^0_{C9} + 0.32p^0_{C6OH}$ (bottom right). The OA, EO, and (CM or CT) beads of the C10E3 surfactant molecules are represented as red, rose, and gray stick models, respectively. The C9 and C6OH additives are shown as green and magenta stick models, respectively. The black rectangle shows the simulation box that is surrounded by partial replicas.

As illustrated in Figure 2, the unary loading data can be described satisfactorily by a quadratic expression:

$$q_{solute} = c_1 p^*_{solute} + c_2 (p^*_{solute})^2 \quad (1)$$

where q_{solute} is the amount of solute adsorbed in the mesophase that is given here as the number ratio (N_{solute}/N_{C10E3}), p_{solute}* is the relative solute pressure ($p_{solute}/p_{solute}{}^0$), and c_1 and c_2 are fitting coefficients. This quadratic expression more closely fits the unary adsorption data than the Freundlich,[46] Langmuir,[47] or Brunauer–Emmett–Teller[48] adsorption isotherms, while still requiring only two parameters (three parameter equations would overfit the five available data points). Talu and Myers[49]

https://doi.org/10.1021/acs.jpcb.2c02871
J. Phys. Chem. B 2022, 126, 3940–3949

highlight the thermodynamic requirement for any adsorption isotherm to have a positive and finite slope in the limit of $p \to 0$ (as described by Henry's law). Equation 1 satisfies this condition, while allowing for curvature at high p through a quadratic term, in order to better fit the data in that regime. Since the mesophase can swell upon solute uptake, there is no requirement for an inflection point leading to a saturation plateau. Instead the isotherm terminates when the surfactant−water−solute system enters the one-phase region. Using eq 1, we obtain the following fitting coefficients: $c_1 = 0.20$ and $c_2 = 0.22$ for C9, and $c_1 = 1.3$ and $c_2 = 0.72$ for C6OH. The c_2/c_1 ratio of the coefficients indicates that the relative curvature (or deviation from the Henry's law region) is more pronounced for C9 than for C6OH.

The loading behavior for the binary mixture as functions of p_{C9}* and p_{C6OH}* is also shown in Figure 2, and numerical data are provided in Table 2. Note that the loading data for $0.64p^0_{C9} + 0.32p^0_{C6OH}$ appear to be outliers; for this combination of high relative pressures, $q_{C9} + q_{C6OH} \approx 1.1$ (i.e., more solute than surfactant molecules are present), and the lamellar phase observed for the finite simulated system may only be metastable with regard to mixing with the reservoir phases (see Figure 3). Nevertheless, also when only the other 24 state points are considered, the simulation data clearly demonstrate a cooperative effect where loading of C9 is enhanced by coadsorption of C6OH and vice versa. However, a cooperative effect is also present for the unary loading as indicated by the positive deviations from Henry's law (i.e., $c_2 > 0$ in eq 1). Thus, the important question is whether the enhancement resulting from C9−C6OH interactions is larger than those resulting from C9−C9 and C6OH−C6OH interactions.

To explain this argument, let us consider the incremental C9 and C6OH loadings normalized by the loading of the other component or pseudocomponent as follows:

$$q_A^{incr}(p_A^*, p_B^*) = [q_A^{binary}(p_A^*, p_B^*) - q_A^{unary}(p_A^*)]/q_B^{unary}(p_B^*) \quad (2)$$

$$q_A^{pseudo}(p_A^*) = [0.5q_A^{unary}(2p_A^*) - q_A^{unary}(p_A^*)] / [0.5q_A^{unary}(2p_A^*)] \quad (3)$$

where the labels "unary" and "binary" indicate the type of system. For the pseudocomponent mixture, one could argue that the denominator in eq 3 should be replaced with $q_A^{unary}(p_A*)$, but we take the conservative approach by normalizing with the larger $0.5q_A^{unary}(2p_A*)$ due to positive deviations from Henry's law. The low uptake at $0.04p^0_{C9}$ and $0.02p^0_{C6OH}$ leads to large statistical uncertainties for these systems. The incremental loading data presented in the bottom part of Figure 2 indicate that the cooperative effect for the C9−C9 pseudomixture is larger than the cooperative effect on C9 loading due to C6OH coadsorption. Interestingly, the opposite holds for the C6OH−C6OH pseudomixture that yields $q^{pseudo}_{C6OH}(p_{C6OH}*)$ values that fall below those due to coadsorption of C9. These observations point to the C9−C9 interactions being most favorable (yielding the largest normalized incremental loading), the C6OH−C6OH interactions being least favorable (but still yielding positive deviations from Henry's law), and the unlike interactions falling in between the like interactions.

The extent of the cooperative effects can also be illustrated through calculation of the Gibbs free energy of transfer from the vapor reservoir to the mesophase that can be obtained from a ratio of number densities that are available as mechanical observables in GEMC simulations:[50,51]

$$\Delta G_{solute}^{vap\to meso} = -RT \log\left(\frac{\rho_{solute}^{meso}}{\rho_{solute}^{ref}}\frac{\rho_{solute}^{ref}}{\rho_{solute}^{vap}}\right) \quad (4)$$

where ρ^{meso}_{solute}, ρ^{vap}_{solute}, and ρ^{ref}_{solute} are the number densities of the solute in the mesophase, the vapor reservoir, and a reference state, respectively. Note that ρ^{ref}_{solute} could be taken as the pure liquid phase of the solute or an ideal gas, but ρ^{ref}_{solute} cancels out in eq 4. Figure 4 shows the Gibbs free energy of transfer for C9 and C6OH solutes at 24 state points (excluding the likely metastable case) as a function of the total number of adsorbed solute molecules (numerical data are provided in Table 2). The Gibbs free energies of transfer for vapor-to-liquid condensation of neat C9 and C6OH are −25.10 ± 0.03 and −21.95 ± 0.01 kJ/mol, respectively, for the SDK model. In comparison, we observe that $\Delta G_{C9}^{vap\to meso}$ ranges from −18.1 to −20.6 kJ/mol; that is, the C9 molecules strongly prefer (by ≈−6 kJ/mol) transfer into their own liquid phase compared to the mesophase. The C6OH molecules also prefer transfer into their own liquid phase but to a lesser extent (by ≈−3 kJ/mol).

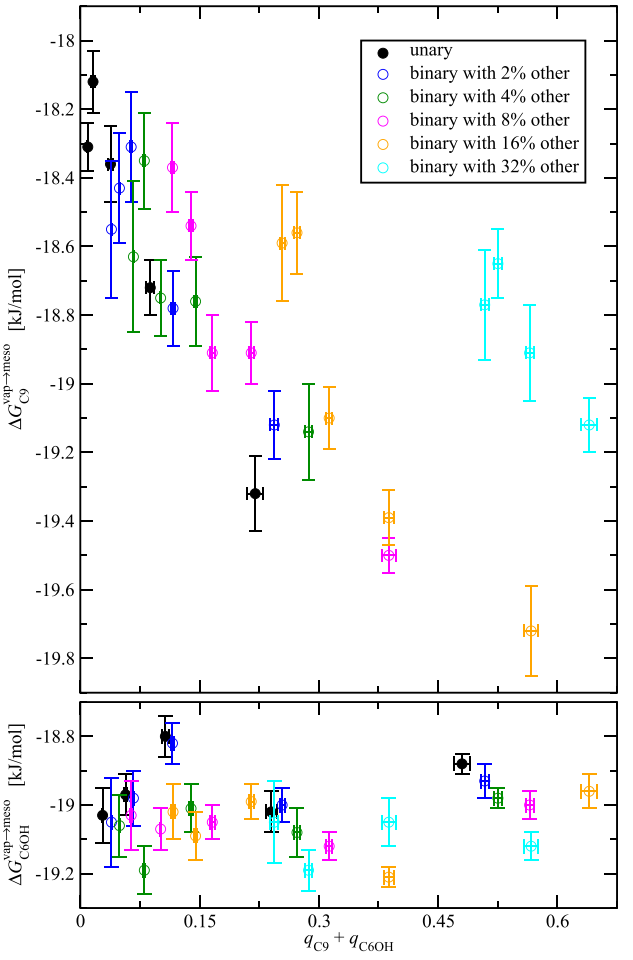

Figure 4. Gibbs free energy of transfer of *n*-nonane (top) and 1-hexanol (bottom) as a function of the total number of solutes per surfactant loaded into the mesophase. Error bars represent the standard error of the mean. Not shown in these graphs are the data for the binary adsorption at $0.64p^0_{C9} + 0.32p^0_{C6OH}$: $\Delta G_{C9}^{vap\to meso}$ = −20.57 ± 0.13 kJ/mol and $\Delta G_{C9}^{vap\to meso}$ = −19.24 ± 0.03 kJ/mol.

https://doi.org/10.1021/acs.jpcb.2c02871
J. Phys. Chem. B 2022, 126, 3940−3949

As illustrated in Figure 4, $\Delta G_{C9}^{vap\rightarrow meso}$ depends significantly on the loading and composition of the mesophase. For unary adsorption, $\Delta G_{C9}^{vap\rightarrow meso}$ decreases from −17.8 to −19.3 kJ/mol as the number of adsorbed C9 molecules increases and the environment becomes more lipophilic. This is consistent with the positive deviation from Henry's law at higher loading (Figure 2); adsorption of additional C9 molecules is more favorable when the bilayer already contains some C9 molecules. In the binary case, a similar trend is found, in which higher total loading leads to more favorable adsorption for C9. However, the rightward shift of the data to higher total loading for increasing p_{C6OH}* indicates that C9−C9 interactions are more favorable than C9−C6OH interactions (see also Figure S1 for data plotted as a function of p*). Consequently, at constant total loading, $\Delta G_{C9}^{vap\rightarrow meso}$ becomes less favorable as the mole fraction of adsorbed C9 molecules decreases.

In contrast to the strong loading dependence observed for $\Delta G_{C9}^{vap\rightarrow meso}$, the $\Delta G_{C6OH}^{vap\rightarrow meso}$ data are scattered in the range from −18.8 to −19.2 kJ/mol, and $\Delta G_{C6OH}^{vap\rightarrow meso}$ does not not vary significantly between unary and binary adsorption nor does it become more favorable with increased total loading. At first hand, these observations appear to conflict with the positive deviations from Henry's law (see Figure 2). However, the different trends in loading and transfer free energy can be reconciled when taking the adsorption-induced swelling of the mesophase into account. The volume of the mesophase, V_{meso} increases from 96 nm^3 without any additive molecules to 122 nm^3 for the system at $0.64p_{C9}^0 + 0.32p_{C6OH}^0$ (see Table 2). The $\Delta G_{solute}^{vap\rightarrow meso}$ values calculated from the ratio of number densities (see eq 4) allows one to correctly separate the effects arising due to interactions with the environment from those that are only a consequence of swelling.[50]

The GEMC simulations also allow for the (calorimetric) determination of the enthalpy of transfer from the difference of partial molar enthalpies: $\Delta H_i^{vap\rightarrow meso} = \underline{H}_i^{vap} - \bar{H}_i^{meso}$. The partial molar enthalpies $\bar{H}_i$ in the mesophase were calculated using multiple linear regression[52] and subtracted from the molar enthalpies computed in the ideal vapor boxes (i.e., accounting only for intramolecular interactions). Due to the large ratio of C10E3 molecules and water beads to additive molecules, the contribution of the additive molecules to the enthalpy of the mesophase is relatively small particularly for low p_{solute}*; hence, the statistical uncertainties are rather large. With the free energies and enthalpies of transfer, the change in entropy upon adsorption in the mesophase can be computed using $\Delta S = (\Delta H - \Delta G)/T$. The values for $\Delta H_i^{vap\rightarrow meso}$ and $\Delta S_i^{vap\rightarrow meso}$ are reported in Figure S2. For the C9 additive, the $\Delta H_{C9}^{vap\rightarrow meso}$ values are scattered around the corresponding enthalpy of condensation for the neat system ($\Delta H_{C9}^{vap\rightarrow liq}$ = −41.17 kJ/mol for the SDK model). In contrast, $\Delta H_{C6OH}^{vap\rightarrow meso}$ values are significantly more favorable than the enthalpy of condensation for the neat C6OH system ($\Delta H_{C6OH}^{vap\rightarrow liq}$ = −36.03 kJ/mol), but the differences diminish as the total loading increases. As should be expected for a transfer from the gas phase to a condensed phase, entropy changes are negative reflecting the entropic cost associated with the formation of a cavity and the solute's hindered translational and rotational motion. Again, the $\Delta S_{C9}^{vap\rightarrow meso}$ values are scattered but, on average, they are about a factor of 1.5 larger in magnitude than the entropy of condensation ($\Delta S_{C9}^{vap\rightarrow liq}$ = −53.6 J/mol·K for the SDK model). The additional entropic cost for transfer into the mesophase signals that the C9 molecules only adsorb in a subregion of the mesophase volume and/or loose part of their rotational entropy during adsorption into the mesophase. For the C6OH additive at low total loading, $\Delta S_{C6OH}^{vap\rightarrow meso}$ values are about 1.7× larger in magnitude than the entropy of condensation ($\Delta S_{C9}^{vap\rightarrow liq}$ = −46.9 J/mol·K for the SDK model), but this difference reduces to a factor of 1.3 at the higher loadings. Both $\Delta H_{C6OH}^{vap\rightarrow meso}$ and $\Delta S_{C6OH}^{vap\rightarrow meso}$ become smaller in magnitude as the loading increases; thus, those changes offset and $\Delta G_{C6OH}^{vap\rightarrow meso}$ remains fairly constant. The C6OH molecules are likely confined to a subregion of space in the mesophase and may exhibit orientational alignment with the C10E3 surfactant molecules forming the bilayer, but the fractional volume of this subregion increases or the orientational confinement becomes less severe as the loading increases. A microscopic analysis of the mesophase structure will be provided in a subsequent section.

Comparison to Ideal Adsorbed Solution Theory. IAST is another way to examine binary adsorption based on unary adsorption data.[7] To compare the loadings observed in the simulations of the binary additive systems to those predicted by IAST, we modified the pyIAST software[53] to incorporate the quadratic expression (eq 1) for the adsorption isotherm. The IAST predictions, q_{solute}^{IAST}, for each of the binary compositions are shown as a function of p* in Figure 2 (and numerical data are provided in Table 2). Figure 5 shows a

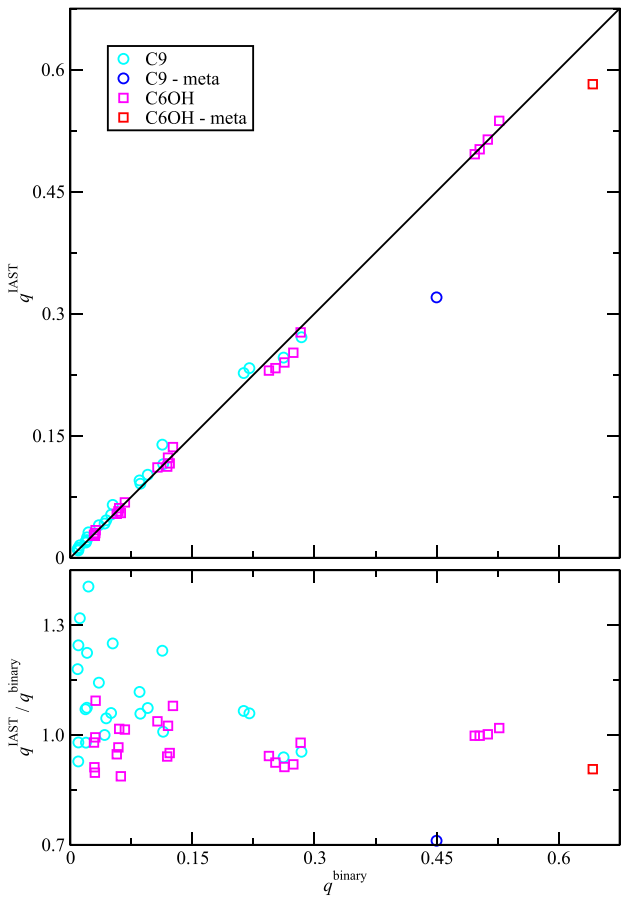

Figure 5. (Top) Scatter plot of the loadings predicted by IAST versus those obtained from the GEMC simulations and (bottom) the corresponding deviation plot. The data for the binary adsorption at $0.64p_{C9}^0 + 0.32p_{C6OH}^0$, where the lamellar phase is likely metastable, are shown in blue and red symbols.

https://doi.org/10.1021/acs.jpcb.2c02871
J. Phys. Chem. B 2022, 126, 3940−3949

scatter plot of q_{solute}^{IAST} versus the GEMC simulation data. With the exception of the C9 and C6OH loadings at $0.64p_{C9}^0$ + $0.32p_{C6OH}^0$, where the mesophase is potentially only metastable, IAST yields remarkably accurate predictions. Excluding the $0.64p_{C9}^0$ + $0.32p_{C6OH}^0$ data, the correlation coefficient and slope for the C9 uptake are 0.995 and 0.984, respectively, and those for the C6OH uptake are 0.999 and 0.997, respectively. Despite the overall satisfactory accuracy of the IAST predictions, IAST clearly over predicts the C9 loadings at $0.32p_{C6OH}^0$ by a factor of ≈1.3 (with the exception of the data point at $0.64p_{C9}^0$). These discrepancies occur when the IAST predictions are extrapolative, requiring spreading pressures in equilibrium with pressures outside the range of the unary adsorption data (p_{C9}* > 0.64). While extrapolation of unary Langmuir-type isotherms for IAST is relatively safe (these exhibit saturation in loading at high pressure),[53] this is less reliable for the quadratic expression used here (eq 1), which does not exhibit saturation. Indeed, a lamellar mesophase will not exhibit a saturation loading, as it can expand to accommodate more adsorbates. Furthermore, the additive loading should diverge near the additive's saturated vapor pressure (as it does in the BET isotherm) or a phase transition to a different mesophase may mark the end of the stability window of the lamellar phase. Such behavior is not captured by the simple quadratic expression used here. Since the C9 loading is much smaller, the IAST predictions for q_{C6OH} do not require significant extrapolation. The agreement between IAST predictions and binary simulations for the C6OH loading supports that C6OH−C6OH and C6OH−C9 interactions are of a similar favorability.

Structural Analysis. Simulation snapshots of the mesophase for four representative binary adsorption systems are shown in Figure 3. These snapshots provide qualitative support for preferential siting of the additive molecules; the C9 molecules prefer locations near the bilayer center but without strong orientational preference, whereas the C6OH molecules are preferentially embedded and aligned with the longer C10E3 molecules. Furthermore, the water region appears to thin with increased additive loading.

Structural data for the bilayer are depicted in Figure 6 (with numerical data provided in Table S4). Uptake of C9 and C6OH molecules leads to an increase of the bilayer thickness (given here as the distance between the two water/leaflet interfaces obtained from a hyperbolic tangent fit to the water density profile), but on a per molecule basis the effect is significantly more prononunced for uptake of C9 molecules than for C6OH molecules. Adsorption at $0.32p_{C9}^0$ + $0.08p_{C6OH}^0$, where q_{C9}^{binary} ≈ q_{C6OH}^{binary} ≈ 0.1 per C10E3 molecule, leads to an increase of ≈8% in the bilayer thickness compared to the bilayer without additives (29.9 Å versus 27.8 Å). While uptake of both additives leads to an increase in bilayer thickness, only uptake of C6OH molecules leads to a significant increase of the area per surfactant molecule, A_{C10E3} (measured here by the cross-sectional area of the orthogonal simulation box divided by the 50 C10E3 molecules per leaflet), whereas the effect from C9 molecules is minimal (i.e., the slope of A_{C10E3} vs p_{C9}* is close to zero). At p_{C6OH}* = 0.16, where q_{C6OH}^{binary} ≈ 0.27 per C10E3 molecule, the relative increase in A_{C10E3} is ≈12% compared to the bilayer without additives; that is, the (partial) cross-sectional area of the C6OH molecules is about a factor of 2 smaller than that of the C10E3 molecules. Uptake of C6OH molecules also leads to a very slight increase in the average end-to-end distance of the C10E3 molecules, whereas the C9

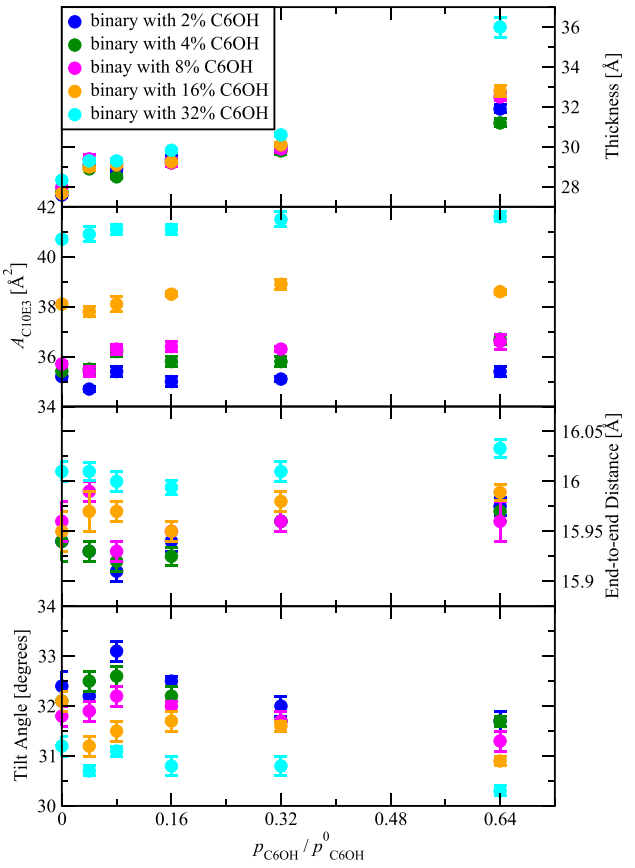

Figure 6. Bilayer thickness (top), area per surfactant molecule (top middle), end-to-end distance of surfactant molecules (bottom middle), and tilt angle of surfactant molecules with respect to the bilayer normal (bottom) vs the relative vapor pressure of the solutes. Error bars represent the standard error of the mean.

molecules have no significant effect. Similarly, uptake of C6OH molecules leads to a small decrease of the C10E3 tilt angle with respect to the bilayer normal, whereas the effect of C9 molecules is minimal. Overall, these trends and the relative impact of C9 and C6OH molecules on structural parameters obtained for the binary adsorption systems are in agreement with the observations for the unary adsorption systems.[37]

As indicated by the increases in A_{C10E3} and the bilayer thickness, the volume of the bilayer box increases with increasing adsorption loading (see also Table 2). Using multiple linear regression,[52] the partial molar volumes $\overline{V}_i$ of each adsorbate can be computed (see Figure S3). Both $\overline{V}_{C9}$ and $\overline{V}_{C6OH}$ are found to be smaller than the molar volumes $\underline{V}_i$ of each solute in their neat liquid phase, indicating that the uptake of both solutes in the mesophase leads to a smaller increase in volume than in their respective liquid phases. For the C9 additives, there is no significant composition dependence and $\overline{V}_{C9}$ ≈ 0.9$\underline{V}_{C9}$. In contrast, $\overline{V}_{C6OH}$ exhibits a small composition dependence with an increase as the additive concentration increases in the mesophase. At intermediate loadings, $\overline{V}_{C6OH}$ is also ≈10% smaller than $\underline{V}_{C6OH}$.

Further information about the mesophase structure can be gleaned from z-resolved density profiles (i.e., along the normal to the bilayer plane). Figure 7 (numerical data are provided in Table S5) shows the density profiles for water, the terminal CT and OA beads of the C10E3 molecules, and the additives' center of mass for unary and binary adsorption systems at

https://doi.org/10.1021/acs.jpcb.2c02871
J. Phys. Chem. B 2022, 126, 3940−3949

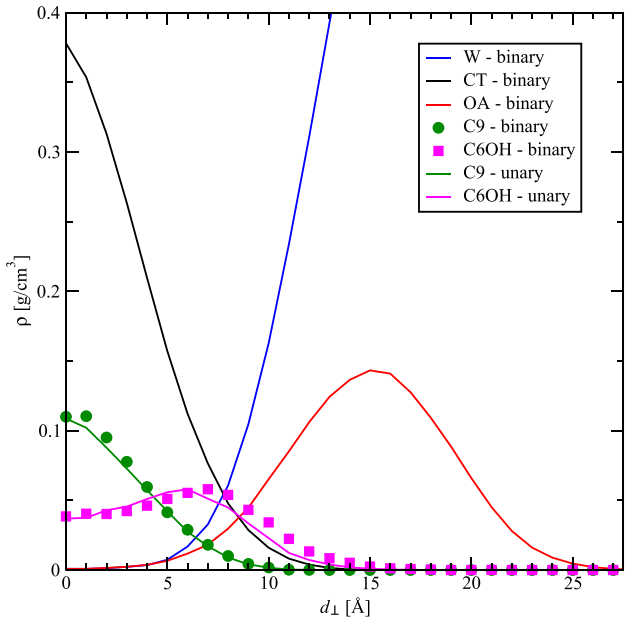

Figure 7. Symmetrized density profiles as a function of position along the bilayer normal for unary (dashed lines) and binary (solid lines) adsorption systems at $0.32p^0_{C9}$ and $0.08p^0_{C6OH}$.

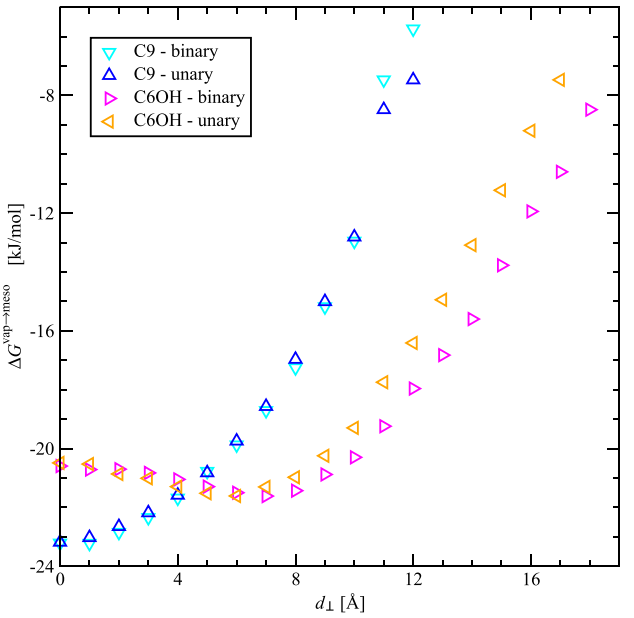

Figure 8. Symmetrized free energy of transfer as a function of solute location along the bilayer normal for unary and binary adsorption systems at $0.32p^0_{C9}$ and $0.08p^0_{C6OH}$.

$0.32p^0_{C9}$ and $0.08p^0_{C6OH}$, where $q^{binary}_{C9} \approx q^{binary}_{C6OH} \approx 0.1$ per C10E3 molecule. It should be noted that our prior work[37] indicated only subtle differences for the OA and CT bead profiles of the C6OH additive. At this moderate loading, the differences between the unary and binary systems are small. C9 molecules load preferentially into the center of the bilayer, while the density profiles for the C6OH molecules show a maximum at $d_\perp$ = 6 and 7 Å for the unary and binary adsorption systems, respectively; that is, the presence of the C9 molecules in the binary systems leads to a slight outward shift in the C6OH profile. Nevertheless, the C6OH molecules also populate the bilayer center for both the unary and binary adsorption systems, and the C6OH density profiles approach zero at the location of the highest OA density for the C10E3 molecules, that is, the C6OH molecules are not located near the outer interface of the bilayer, but are still in contact with water molecules penetrating into the polar region of the C10E3 surfactants.

Using the number densities corresponding to the additives' center-of-mass profiles, eq 4 can also be applied to obtain the free energy of transfer into different regions of the mesophase (see Figure 8 and Table S6). Again, we take the unary and binary adsorption systems at $0.32p^0_{C9}$ and $0.08p^0_{C6OH}$ as a representative example. As should be expected from the bead density profiles, the differences between the unary and binary adsorption system are negligible with the exception of the slight outward shift for the free energy minimum for the C6OH additive in the binary system. At this state point for the binary adsorption system, the free energy values for the entire mesophase are $\Delta G^{vap\to meso}_{C9} = -18.9$ kJ/mol and $\Delta G^{vap\to meso}_{C6OH} = -19.0$ kJ/mol (see Table 2). For the C9 molecules, $\Delta G^{vap\to meso}_{C9}(z)$ is most favorable in the center of the bilayer with a value of −23.2 kJ/mol and remains below −18.9 kJ/mol for $d_\perp$ < 7 Å. However, not even the center of the bilayer can provide an environment as favorable as C9's neat liquid phase ($\Delta G^{vap\to liq}_{C9} = -25.10$ kJ/mol). In contrast, the most favorable location for the C6OH at $d_\perp$ = 7 Å yields $\Delta G^{vap\to meso}_{C6OH}(z)$ = −21.6 kJ/mol, which approaches the value for C6OH's neat liquid phase ($\Delta G^{vap\to liq}_{C6OH} = -21.95$ kJ/mol). At the outer interface of the bilayer ($d_\perp$ = 15 Å, the preferred location of the surfactant's OA bead), $\Delta G^{vap\to meso}_{C6OH}(z)$ has already increased by 8 kJ/mol compared to the minimum, whereas the bilayer center is only less favorable by 1 kJ/mol than the minimum.

CONCLUSIONS

Thermodynamic and molecular-level information on the binary uptake of *n*-nonane and 1-hexanol molecules in the lamellar phase formed by nonpolar C10E3 surfactants is obtained through Monte Carlo simulations in the osmotic Gibbs ensemble. These simulations allow us to assess the hypothesis that different spatial preferences of nonpolar and amphiphilic solutes should lead to synergistic uptake beyond that expected from unary adsorption. The differences in spatial preferences observed previously for unary adsorption systems[37] are found to be preserved for the binary adsorption system; that is, C9 molecules adsorb preferentially near the bilayer center and cause an increase in the bilayer thickness, whereas C6OH molecules preferentially embed near the intersection of nonpolar and polar beads of the C10E3 surfactants and cause an increase in the bilayer area. However, analysis of the composition-dependent free energy of transfer indicates that an increase in the C9 loading leads to a more favorable mesophase environment for additional C9 molecules, whereas the transfer free energy for C6OH molecules is fairly independent of composition. Similarly, comparison to predictions made using Ideal Adsorbed Solution Theory and to loadings estimated for pseudobinary mixtures point to C9−C6OH interactions being less favorable than C9−C9 interactions, but the former are close to C6OH−C6OH interactions. Although we observe positive deviations from Henry's law for the adsorption of both C9 and C6OH molecules when expressed per surfactant molecule, the swelling of the mesophase partially or fully compensates when considering the Gibbs free energies of transfer for C9 or

https://doi.org/10.1021/acs.jpcb.2c02871
J. Phys. Chem. B 2022, 126, 3940−3949

C6OH molecules, respectively. The reason is that, for C9 molecules, its own liquid phase provides a solvation environment that is more favorable than the mesophase by about 6 kJ/mol, whereas the difference is only about 3 kJ/mol for the C6OH molecules. Thus, the C9 molecules have more to gain when other C9 molecules are adsorbed. For the C9 molecules, the enthalpy of adsorption into the mesophase is close to the enthalpy of condensation into its neat liquid phase, but the entropic cost of transferring into a relatively small subregion of the mesophase is significantly larger than that of condensation. In contrast, the mesophase provides a more favorable enthalpy of transfer for the C6OH molecules compared to its neat liquid phase, but the increase in entropic cost for transfer into the mesophase more than compensates. Overall, our simulation study demonstrates that different spatial preferences for the loading of different additives do not necessarily result in synergistic effects for binary adsorption beyond those observed in the unary adsorption systems.

■ ASSOCIATED CONTENT

Supporting Information

The Supporting Information is available free of charge at https://pubs.acs.org/doi/10.1021/acs.jpcb.2c02871.

Additional force field details (nonbonded interaction parameters, bond stretching parameters, and angle bending parameters); Tables with numerical data for Figures 6, 7, and 8; Figures showing additive free energies as a function of partial pressure, enthalpies and entropies as a function of loading, and partial molar volumes as a function of reduced pressure (PDF)

■ AUTHOR INFORMATION

Corresponding Authors

Mona S. Minkara − *Department of Bioengineering, Northeastern University, Boston, Massachusetts 02115, United States; Department of Chemistry and Chemical Theory Center, University of Minnesota, Minneapolis, Minnesota 55455-0431, United States;* orcid.org/0000-0003-1821-2725; Email: m.minkara@northeastern.edu

J. Ilja Siepmann − *Department of Chemistry and Chemical Theory Center, University of Minnesota, Minneapolis, Minnesota 55455-0431, United States; Department of Chemical Engineering and Materials Science, University of Minnesota, Minneapolis, Minnesota 55455-0132, United States;* orcid.org/0000-0003-2534-4507; Email: siepmann@umn.edu

Authors

Tyler R. Josephson − *Department of Chemistry and Chemical Theory Center, University of Minnesota, Minneapolis, Minnesota 55455-0431, United States; Department of Chemical, Biochemical, and Environmental Engineering, University of Maryland, Baltimore, Maryland 21250, United States*

Connor L. Venteicher − *Department of Chemistry and Chemical Theory Center, University of Minnesota, Minneapolis, Minnesota 55455-0431, United States*

Benjamin R. Greenvall − *Department of Bioengineering, Northeastern University, Boston, Massachusetts 02115, United States;* orcid.org/0000-0003-3758-6802

Rebecca K. Lindsey − *Department of Chemistry and Chemical Theory Center, University of Minnesota, Minneapolis, Minnesota 55455-0431, United States;* orcid.org/0000-0002-3438-9064

Peter H. Koenig − *Computational Chemistry, Modeling and Simulation, The Procter and Gamble Company, West Chester, Ohio 45069, United States;* orcid.org/0000-0002-6512-5686

Complete contact information is available at: https://pubs.acs.org/10.1021/acs.jpcb.2c02871

Notes

The authors declare no competing financial interest.

■ ACKNOWLEDGMENTS

This research was partially supported by the National Science Foundation through Awards CBET-1159837 (M.S.M., R.K.L., and J.I.S.) and OAC-1835067 (M.S.M. and J.I.S.), the U.S. Department of Energy, Office of Basic Energy Sciences, Division of Chemical Sciences, Geosciences and Biosciences under Award DE-FG02-17ER16362 (T.R.J. and J.I.S.), the Procter and Gamble Company (M.S.M. and R.K.L.), and the University of Minnesota Disability Resource Center for C.L.V. and additional access assistants for Dr. Minkara (specifically, Tanner Lambson, Natalie Guse, and Alex McKeever). Computer resources were provided by the Minnesota Supercomputing Institute. Support for B.R.G. during the writing phase of this manuscript was provided by Northeastern University.

■ REFERENCES

(1) Rane, S. S.; Anderson, B. D. What Determines Drug Solubility in Lipid Vehicles: Is It Predictable? *Adv. Drug Delivery Rev.* **2008**, *60*, 638−656.

(2) Lawrence, M. J. Surfactant Systems: Their Use in Drug Delivery. *Chem. Soc. Rev.* **1994**, *23*, 417−424.

(3) Somasundaran, P.; Chakraborty, S.; Qiang, Q.; Deo, P.; Wang, J.; Zhang, R. Surfactants, Polymers, and Their Nanoparticles for Personal Care Applications. *J. Cosmet. Sci.* **2004**, *55*, S1−S17.

(4) Williams, H. D.; Trevaskis, N. L.; Charman, S. A.; Shanker, R. M.; Charman, W. N.; Pouton, C. W.; Porter, C. J. H. Strategies to Address Low Drug Solubility in Discovery and Development. *Pharmacol. Rev.* **2013**, *65*, 315−499.

(5) Raffa, P.; Broekhuis, A. A.; Picchioni, F. Polymeric Surfactants for Enhanced Oil Recovery: A Review. *J. Petrol. Sci. Eng.* **2016**, *145*, 723−733.

(6) Siepmann, J. I.; Brennecke, J. F.; Allen, D. T.; Klein, M. T.; Savage, P. E.; Schatz, G. C.; Winnik, F. M. ACS Virtual Issue on Multicomponent Systems: Absorption, Adsorption, and Diffusion. *J. Chem. Eng. Data* **2018**, *63*, 3651.

(7) Myers, A. L.; Prausnitz, J. M. Thermodynamics of Mixed-Gas Adsorption. *AIChE J.* **1965**, *11*, 121−127.

(8) Hand, D. W.; Loper, S.; Ari, M.; Crittenden, J. C. Prediction of Multicomponent Adsorption Equilibria Using Ideal Adsorbed Solution Theory. *Environ. Sci. Technol.* **1985**, *19*, 1037−1043.

(9) Walton, K. S.; Sholl, D. S. Predicting Multicomponent Adsorption: 50 years of the Ideal Adsorbed Solution Theory. *AIChE J.* **2015**, *61*, 2757−2762.

(10) Bai, P.; Tsapatsis, M.; Siepmann, J. I. Multicomponent Adsorption of Alcohols onto Silicalite-1 from Aqueous Solution: Isotherms, Structural Analysis, and Assessment of Ideal Adsorbed Solution Theory. *Langmuir* **2012**, *28*, 15566−15576.

(11) Ali, A. A.; Mulley, B. A. Formation of Liquid Crystal and Other Non-Fluid Phases in Emulsions Containing Non-Ionic Surfactants. *J. Pharm. Pharmacol.* **2011**, *30*, 205−213.

(12) Mitchell, D. J.; Tiddy, G. J. T.; Waring, L.; Bostock, T.; McDonald, M. P. Phase Behaviour of Polyoxyethylene Surfactants

with Water. Mesophase Structures and Partial Miscibility (Cloud Points). *J. Chem. Soc., Faraday Trans.1* **1983**, *79*, 975−1000.
(13) Nagarajan, R. Solubilization by Amphiphilar Aggregates. *Curr. Opin. Colloid Interface Sci.* **1997**, *2*, 282−293.
(14) Le, T. D.; Olsson, U.; Mortensen, K.; Zipfel, J.; Richtering, W. Nonionic Amphiphilic Bilayer Structures under Shear. *Langmuir* **2001**, *17*, 999−1008.
(15) Ward, A. J. I.; Ku, H.; Phillippi, M. A.; Marie, C. Order of Polyoxyethylene Chains in the Lamellar Phase of a Nonionic Surfactant. *Mol. Cryst. Liq. Cryst.* **1988**, *154*, 55−60.
(16) Schönhoff, M.; Söderman, O.; Li, Z. X.; Thomas, R. K. Internal Dynamics and Order Parameters in Surfactant Aggregates: A 2H NMR Study of Adsorption Layers and Bulk Phases. *Langmuir* **2000**, *16*, 3971−3976.
(17) Ferreira, T. M.; Medronho, B.; Martin, R. W.; Topgaard, D. Segmental Order Parameters in a Nonionic Surfactant Lamellar Phase Studied with $^{1}H-^{13}C$ Solid-State NMR. *Phys. Chem. Chem. Phys.* **2008**, *10*, 6033−6038.
(18) Klose, G.; Eisenblätter, S.; Galle, J.; Islamov, A.; Dietrich, U. Hydration and Structural Properties of a Homologous Series of Nonionic Alkyl Oligo(ethylene oxide) Surfactants. *Langmuir* **1995**, *11*, 2889−2892.
(19) Sottmann, T.; Strey, R.; Chen, S.-H. A Small-Angle Neutron Scattering Study of Nonionic Surfactant Molecules at the Water−Oil Interface: Area per Molecule, Microemulsion Domain Size, and Rigidity. *J. Chem. Phys.* **1997**, *106*, 6483−6491.
(20) Nilsson, P. G.; Lindman, B. Water Self-Diffusion in Nonionic Surfactant Solutions. Hydration and Obstruction Effects. *J. Phys. Chem.* **1983**, *87*, 4756−4761.
(21) Katz, Y.; Diamond, J. M. A Method for Measuring Nonelectrolyte Partition Coefficients Between Liposomes and Water. *J. Membr. Biol.* **1974**, *17*, 69−86.
(22) Rowe, E.; Zhang, F.; Leung, T.; Parr, J.; Guy, P. Thermodynamics of Membrane Partitioning for a Series of n-Alcohols Determined by Titration Calorimetry: Role of Hydrophobic Effects. *Biochemistry* **1998**, *37*, 2430−2440.
(23) Larson, R. G. Monte Carlo Simulation of Microstructural Transitions in Surfactant Systems. *J. Chem. Phys.* **1992**, *96*, 7904−7918.
(24) Karaborni, S.; van Os, N. M.; Esselink, K.; Hilbers, P. A. J. Molecular Dynamics Simulations of Oil Solubilization in Surfactant Solutions. *Langmuir* **1993**, *9*, 1175−1178.
(25) Pedersen, U. R.; Peters, G. H.; Westh, P. Molecular Packing in 1-Hexanol−DMPC Bilayers Studied by Molecular Dynamics Simulation. *Biophys. Chem.* **2007**, *125*, 104−111.
(26) Dickey, A. N.; Faller, R. How Alcohol Chain-Length and Concentration Modulate Hydrogen Bond Formation in a Lipid Bilayer. *Biophys. J.* **2007**, *92*, 2366−2376.
(27) Dickey, A. N.; Yim, W.-S.; Faller, R. Using Ergosterol to Mitigate the Deleterious Effects of Ethanol on Bilayer Structure. *J. Phys. Chem. B* **2009**, *113*, 2388−2397.
(28) Rane, S. S.; Anderson, B. D. Molecular Dynamics Simulations of Functional Group Effects on Solvation Thermodynamics of Model Solutes in Decane and Tricaprylin. Mol. *Pharmaceutics* **2008**, *5*, 1023−1036.
(29) Woodhead, J. L.; Hall, C. K. Simulation of Micelle Formation in the Presence of Solutes. *Langmuir* **2010**, *26*, 15135−15141.
(30) Denham, N.; Holmes, M. C.; Zvelindovsky, A. V. The Phases in a Non-Ionic Surfactant ($C_{12}E_6$)−Water Ternary System: A Coarse-Grained Computer Simulation. *J. Phys. Chem. B* **2011**, *115*, 1385−1393.
(31) Sanders, S. A.; Sammalkorpi, M.; Panagiotopoulos, A. Z. Atomistic Simulations of Micellization of Sodium Hexyl, Heptyl, Octyl, and Nonyl Sulfates. *J. Phys. Chem. B* **2012**, *116*, 2430−2437.
(32) Ludwig, J.; Maibaum, L. Effects of Alcohol on the Phase Separation in Model Membranes. *Chem. Phys. Lipids* **2020**, *233*, 104986.
(33) Floriano, M. A.; Caponetti, E.; Panagiotopoulos, A. Z. Micellization in Model Surfactant Systems. *Langmuir* **1999**, *15*, 3143−3151.
(34) Rekvig, L.; Frenkel, D. Molecular Simulations of Droplet Coalescence in Oil/Water/Surfactant Systems. *J. Chem. Phys.* **2007**, *127*, 134701.
(35) Rodgers, J. M.; Webb, M.; Smit, B. Alcohol Solubility in a Lipid Bilayer: Efficient Grand-Canonical Simulation of an Interfacially Active Molecule. *J. Chem. Phys.* **2010**, *132*, 064107.
(36) Panagiotopoulos, A. Z.; Quirke, N.; Stapleton, M.; Tildesley, D. J. Phase Equilibria by Simulation in the Gibbs Ensemble. *Mol. Phys.* **1988**, *63*, 527−545.
(37) Minkara, M. S.; Lindsey, R. K.; Hembree, R. H.; Venteicher, C. L.; Jamadagni, S. N.; Eike, D. M.; Ghobadi, A. F.; Koenig, P. H.; Siepmann, J. I. Probing Additive Loading in the Lamellar Phase of a Nonionic Surfactant: Gibbs Ensemble Monte Carlo Simulations Using the SDK Force Field. *Langmuir* **2018**, *34*, 8245−8254.
(38) Siepmann, J. I.; Martin, M. G.; Chen, B.; Wick, C. D.; Stubbs, J. M.; Potoff, J. J.; Eggimann, B. L.; McGrath, M. J.; Zhao, X. S.; Anderson, K. E.; et al. *Monte Carlo for Complex Chemical Systems—Minnesota, V19*; University of Minnesota: Minneapolis, MN, 2019.
(39) Shinoda, W.; DeVane, R.; Klein, M. L. Multi-Property Fitting and Parameterization of a Coarse Grained Model for Aqueous Surfactants. *Mol. Simul.* **2007**, *33*, 27−36.
(40) Shinoda, W.; DeVane, R.; Klein, M. L. Coarse-Grained Molecular Modeling of Non-Ionic Surfactant Self-Assembly. *Soft Matter* **2008**, *4*, 2454−2462.
(41) Shinoda, W.; DeVane, R.; Klein, M. L. Zwitterionic Lipid Assemblies: Molecular Dynamics Studies of Monolayers, Bilayers, and Vesicles Using a New Coarse Grain Force Field. *J. Phys. Chem. B* **2010**, *114*, 6836−6849.
(42) Kemme, H. R.; Kreps, S. I. Vapor Pressure of Primary n-Alkyl Chlorides and Alcohols. *J. Chem. Eng. Data* **1969**, *14*, 98−102.
(43) Martínez, L.; Andrade, R.; Birgin, E. G.; Martínez, J. M. PACKMOL: A Package for Building Initial Configurations for Molecular Dynamics Simulations. *J. Comput. Chem.* **2009**, *30*, 2157−2164.
(44) Mooij, G. C. A. M.; Frenkel, D.; Smit, B. Direct Simulation of Phase Equilibria of Chain Molecules. *J. Phys.: Condens. Matter* **1992**, *4*, L255−L259.
(45) Martin, M. G.; Siepmann, J. I. Novel Configurational-Bias Monte Carlo Method for Branched Molecules. Transferable Potentials for Phase Equilibria. 2. United-Atom Description for Branched Alkanes. *J. Phys. Chem. B* **1999**, *103*, 4508−4517.
(46) Freundlich, H. Über die Adsorption in Lösungen. *Z. Phys. Chem.* **1906**, *57*, 385−470.
(47) Langmuir, I. The Adsorption of Gases on Plane Surfaces of Glass, Mica and Platinum. *J. Am. Chem. Soc.* **1918**, *40*, 1361−1403.
(48) Brunauer, S.; Emmett, P. H.; Teller, E. Adsorption of Gases in Multimolecular Layers. *J. Am. Chem. Soc.* **1938**, *60*, 309−319.
(49) Talu, O.; Myers, A. L. Rigorous Thermodynamic Treatment of Gas Adsorption. *AIChE J.* **1988**, *34*, 1887−1893.
(50) Ben-Naim, A.; Mazo, R. Size Dependence of Solvation Gibbs Energies: A Critique and a Rebuttal of Some Recent Publications. *J. Phys. Chem. B* **1997**, *101*, 11221−11225.
(51) Martin, M. G.; Siepmann, J. I. Calculating Gibbs Free Energies of Transfer from Gibbs Ensemble Monte Carlo Simulations. *Theor. Chem. Acc.* **1998**, *99*, 347−350.
(52) Josephson, T. R.; Singh, R.; Minkara, M. S.; Fetisov, E. O.; Siepmann, J. I. Partial Molar Properties from Molecular Simulation Using Multiple Linear Regression. *Mol. Phys.* **2019**, *117*, 3589−3602.
(53) Simon, C. M.; Smit, B.; Haranczyk, M. pyIAST: Ideal Adsorbed Solution Theory (IAST) Python Package. *Comput. Phys. Commun.* **2016**, *200*, 364−380.

https://doi.org/10.1021/acs.jpcb.2c02871
J. Phys. Chem. B 2022, 126, 3940−3949